Research Article | Vol. 30, No. 13 / 20 Jun 2022 / Optics Express 23260
Optics EXPRESS

Membrane multiple quantum well electro-optical modulator employing low loss high-k radio-frequency slot waveguides

JIANGHAO XING,[1] CHANGZHENG SUN,[1,2,*] BING XIONG,[1,2] JIAN WANG,[1,2] ZHIBIAO HAO,[1,2] LAI WANG,[1] YANJUN HAN,[1,2,3] HONGTAO LI,[1] AND YI LUO[1,2,3]

[1]*Beijing National Research Centre for Information Science and Technology (BNRist), Department of Electronic Engineering, Tsinghua University, Beijing, 100084, China*
[2]*Center for Flexible Electronics Technology, Tsinghua University, Beijing, 100084, China*
[3]*Flexible Intelligent Optoelectronic Device and Technology Center, Institute of Flexible Electronics Technology of THU, Jiaxing Zhejiang, 314000, China*
[*]*czsun@tsinghua.edu.cn*

Abstract: A membrane multiple quantum well (MQW) electro-optical (EO) modulator exploiting low loss high-k radio-frequency (RF) slot waveguides is proposed for sub-terahertz bandwidth. By employing high-k barium titanate (BTO) claddings in place of doped InP cladding layers in traditional InP-based MQW modulators, the proposed modulator exhibits enhanced modulation efficiency and bandwidth as well as reduced insertion loss. A low half-wave voltage-length product of 0.24 V·cm is estimated, together with over 240 GHz bandwidth for a 2-mm-long modulation region, thus allowing sub-terahertz operation.

1. Introduction

High-speed EO Mach-Zehnder modulators (MZMs) play an important role in optical communications [1–3] and microwave photonics [4]. High performance modulators are required in such applications, including small half-wave voltage V_π, low insertion loss, short modulation length and large modulation bandwidth. In practice, however, these requirements are usually contradictory and difficult to fulfill simultaneously. Commonly used materials for EO MZMs include organic polymers, silicon, lithium niobate (LN) and III-V compound semiconductors. Thanks to the high EO coefficient of organic polymers, a polymer EO modulator based on metal-insulator-metal (MIM) structure can be as short as only tens of microns, while its theoretical modulation bandwidth can reach ~THz [5–7]. However, such devices suffer from high insertion loss due to significant optical absorption loss induced by the MIM structure. Silicon-based modulators exploit plasma dispersion effect due to the absence of Pockels effect. The modulation bandwidth of carrier-injection devices is limited by carrier transit time [8], while carrier-depletion devices exhibit low modulation efficiency [9–12]. Thin-film LN (TFLN) modulators have attracted extensive research interest in recent years [2,13–17]. However, so far, the half-wave voltage-length product $V_\pi L$ of the reported TFLN modulators remains ~2 V·cm due to low electric field loading efficiency, which is defined as the ratio of the voltage falling on active region to the total applied voltage. In III-V compound semiconductors, Pockels and Kerr effects, as well as quantum-confined Stark effect (QCSE) in multiple-quantum-wells (MQWs) can be exploited for efficient modulation [18–21]. The MQW core of InP-based modulators exhibit high electric field loading efficiency and typical $V_\pi L$ is ~0.6 V·cm. InP MZMs based on n-i-p-n heterostructure have demonstrated half-wave voltage of 1.5 V and 3-dB modulation bandwidth exceeding 60 GHz [22,23]. Nevertheless, the doped cladding layers in InP-based modulators

#460293 https://doi.org/10.1364/OE.460293
Journal © 2022 Received 5 Apr 2022; revised 4 May 2022; accepted 2 Jun 2022; published 10 Jun 2022

Optics EXPRESS

cause additional microwave loss, which limit their modulation bandwidth. The best modulation bandwidth performance of InP-based modulators reported so far is around 80 GHz [23].

In this work, we propose a novel membrane MQW EO modulator, which combines tight optical confinement of photonic waveguides with high electric field loading efficiency of low loss high-k RF slot waveguides [24]. Adopting high-k material BTO as the cladding layers significantly improves the optical and electrical properties of the device. The high refractive index contrast between the BTO claddings and the MQW core ensures strong optical confinement, while the enormous dielectric constant of the BTO claddings results in efficient electric field loading in the MQW core. Meanwhile, the highly insulating BTO not only avoids free carrier absorption loss due to the doped claddings in traditional InP-based modulators, but also helps greatly reduce the microwave loss. Consequently, the proposed modulator structure exhibits both improved modulation bandwidth and high modulation efficiency, as well as reduced insertion loss. Simulation results reveal that the membrane MQW modulator with a 2-mm-long modulation region exhibits a half-wave voltage of 1.2 V and a bandwidth over 240 GHz.

2. Device structure

The 3D schematic as well as the cross-sectional and top views of the proposed membrane MQW EO modulator are illustrated in Fig. 1. The membrane modulator contains a 390-nm-thick MQW core consisting of 19 pairs of 10 nm/10 nm InGaAlAs/InAlAs quantum wells [1] sandwiched between BTO cladding layers. The MQW core can be formed via transfer-print [25,26] or bonding technique [27,28], whereas the BTO claddings can be prepared with RF magnetron sputtering followed by a lift-off process. The effective dielectric constant and conductivity of sputtered BTO is reported to be 210 and 9.1×10^{-11} S/cm, respectively [29], while its refractive index is 1.85 at a wavelength of 1550 nm. Compared with InP claddings commonly adopted in InP-based MQW modulators, BTO claddings not only ensures strong EO interaction, but also suppresses microwave propagation loss and optical absorption loss.

In an n-i-p-n MQW modulator, the doped InP cladding layers form resistively coupled MQW (RC-MQW) loop, ensuring efficient loading of the electric field to the MQW core, as shown in Figs. 2(a) and 2(b). However, the doped claddings induce additional RF loss, making it difficult to further increase the bandwidth of traditional InP-based modulators. The optical field distribution in the n-i-p-n MQW modulator is given in Fig. 2(c). A portion of the optical field is seen to penetrate into the doped claddings due to the relatively small refractive index contrast between the cladding layers (n_{InP} = 3.17) and the MQW core (n_{MQW} = 3.37), resulting in free carrier absorption loss. In the proposed membrane modulator, high-k material BTO is adopted in place of doped InP claddings to form a capacitively coupled MQW (CC-MQW) loop, as shown in Fig. 2(d). As the dielectric constant of BTO (ε_{BTO} = 210) is much greater than that of the MQW core (ε_{MQW} = 12.256), the continuity of electric displacement vector along z-direction means highly concentrated RF field in the MQW core. In other words, the formation of high-k RF slotline [30] ensures efficient loading of the RF modulation field, as shown in Fig. 2(e). Meanwhile, the low conductivity of BTO helps reduce microwave loss while maintaining high electric field loading efficiency, thus allowing further improvement of the modulation bandwidth. The high refractive index contrast between the BTO claddings (n_{BTO} = 1.85) and the MQW core enables a strong optical confinement in the membrane modulator, as shown in Fig. 2(f). A tight optical confinement means enhanced EO interaction, which is conducive to half-wave voltage reduction. In addition, the highly insulating BTO eliminates free carrier absorption loss, resulting in reduced insertion loss.

Optics EXPRESS

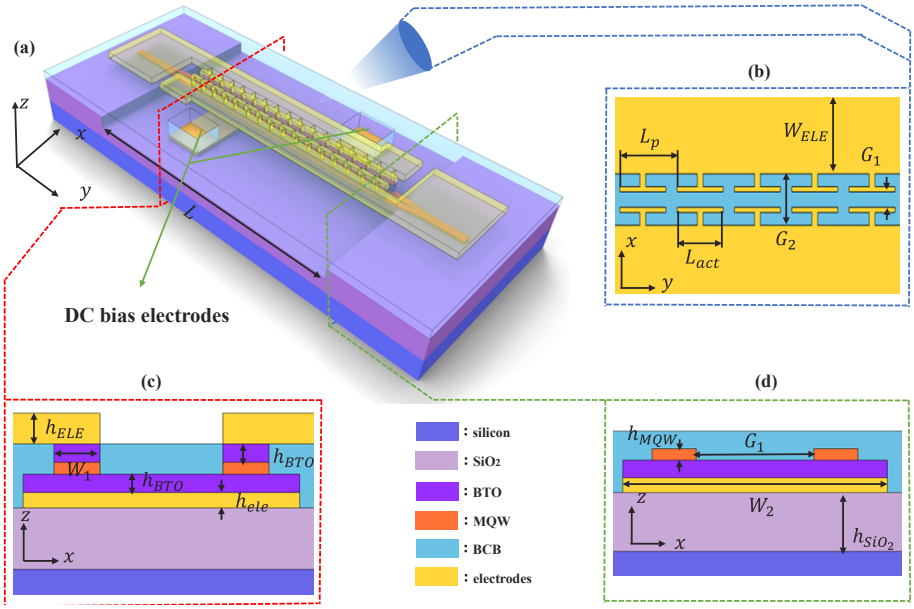

Fig. 1. (a) 3D schematic view, (b) top view and cross-sectional view of (c) loaded region and (d) unloaded region of the membrane MQW EO modulator.

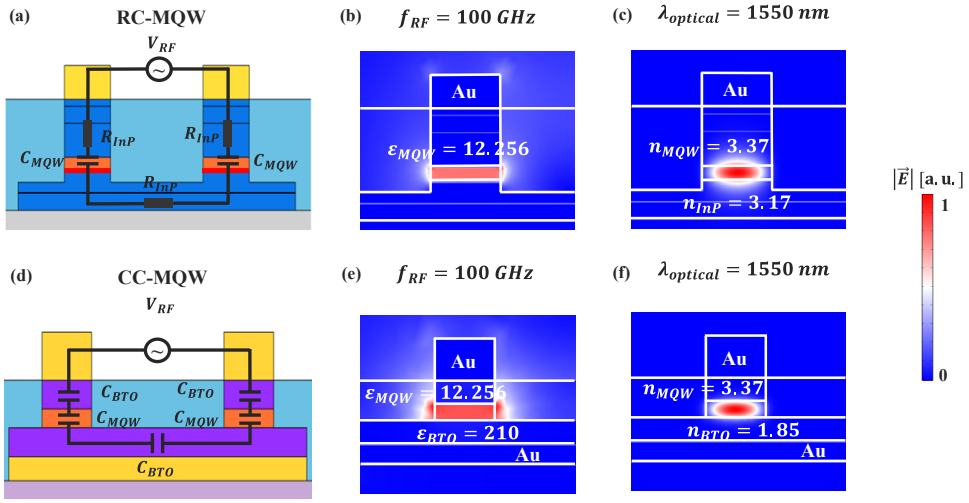

Fig. 2. (a) RC-MQW loop, (b) RF field and (c) optical field within an n-i-p-n modulator. (d) CC-MQW loop, (e) RF field and (f) optical field within the membrane modulator

Optics EXPRESS

3. Design of the membrane MQW modulator

3.1. Waveguide structure

As depicted in Fig. 1(c), the waveguide width W_1 is set to 1.5 μm to ensure single mode operation while taking fabrication feasibility into consideration. The gap G_1 between the two modulation arms is taken to be 4 μm. The variation of the optical absorption loss and the electric field loading efficiency with the BTO cladding thickness h_{BTO} is shown in Fig. 3. The optical absorption loss increases abruptly when h_{BTO} is below 200 nm, as the evanescent optical field in the BTO cladding layer becomes in contact with the gold electrodes, while it remains basically unvaried when h_{BTO} is greater than 400 nm. On the other hand, the electric field loading efficiency decreases with h_{BTO}, as a greater portion of the modulation voltage falls on the BTO claddings. In order to satisfy both high electric field loading efficiency and low optical absorption loss, h_{BTO} is determined to be 400 nm.

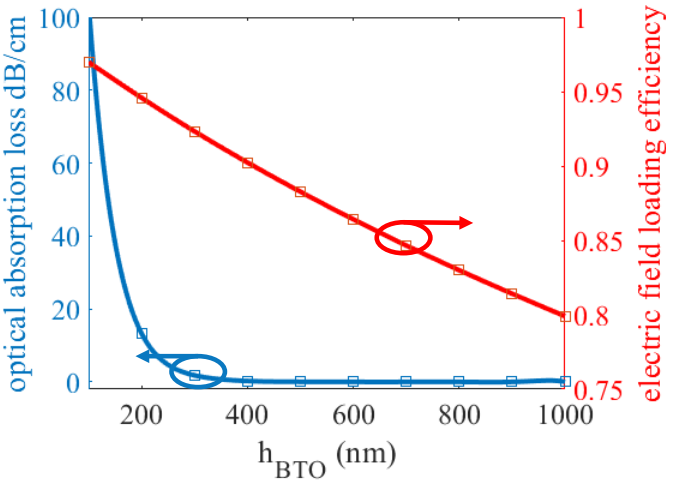

Fig. 3. Variation of optical absorption loss and electric field loading efficiency with h_{BTO}.

3.2. Design of the CL-TWEs

Capacitance-loaded traveling-wave electrodes (CL-TWEs) is employed to ensure excellent impedance matching and velocity matching, as shown in Fig. 1(b). The T-rails in CL-TWEs allow independent adjustment of capacitance and inductance per unit length [31]. The capacitance per unit length mainly depends on the T-rails, while the inductance per unit length can be adjusted by varying the width and the gap of the main electrodes. For InP-based MQW modulators with doped InP claddings, a secondary epitaxy or ion implantation process is required to implement the CL-TWEs. In the proposed membrane modulator, electrical isolation between the loaded region and the unloaded region can be directly realized by the highly insulating benzocyclobutene (BCB) and BTO.

For the 390-nm-thick MQW core, the duty cycle of T-rails η should be around 0.8 to ensure desired value of the capacitance per unit length (233.33 pF/m). The gap G_2 and width W_{ELE} of the main electrodes need to be adjusted to obtain the expected value of inductance per unit length (583.33 nH/m). A wide main electrode helps reduce microwave loss, thus improving the modulation performance. Based on our simulations, W_{ELE} is taken to be 20 μm, as further widening of the main electrodes does not lead to noticeable decrease in microwave loss. The corresponding G_2 is determined to be 12 μm. The period of the CL-TWE is chosen to be 50

Optics EXPRESS

μm to ensure a cut-off frequency (Bragg frequency) beyond 500 GHz. The modulation length is taken as 2 mm to obtain high modulation bandwidth and low half-wave voltage at the same time. The optimized parameters of the membrane modulator are listed in Table 1.

Table 1. Parameters of the proposed membrane MQW EO modulator

Parameter	L	h_{ELE}	h_{ele}	h_{BTO}	h_{SiO2}	h_{MQW}
Value	2 mm	2 μm	500 nm	400 nm	3 μm	390 nm
Parameter	W_1	W_2	G_1	G_2	W_{ELE}	η
Value	1.5 μm	9 μm	4 μm	12 μm	20 μm	0.8

4. Results and discussion

4.1. Microwave loss, electric filed loading efficiency and optical absorption loss

The calculated microwave loss per effective modulation length of the membrane MQW modulator through a full-wave simulation is shown in Fig. 4, in which the microwave loss of the n-i-p-n modulator is also plotted for comparison. The dielectric loss tangents for BTO, silicon, SiO_2 and BCB are set to 3×10^{-2} [30], 3×10^{-5}, 2×10^{-3} and 1×10^{-2}, respectively. At low frequencies, the microwave losses of the two modulators are basically equal. As the modulation frequency increases, microwave loss due to the doped claddings become dominant, and the n-i-p-n modulator exhibits a much higher microwave loss at frequencies above 100 GHz.

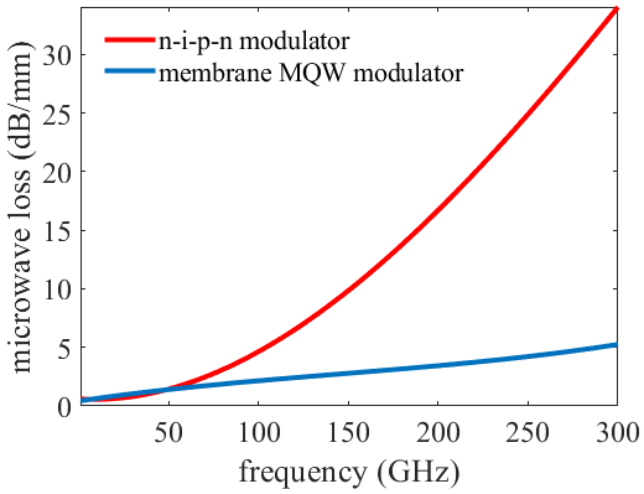

Fig. 4. Microwave loss per effective modulation length of the membrane MQW modulator and the n-i-p-n modulator.

Finite element method (FEM) is employed to evaluate the distribution of optical and microwave fields in the devices. Triangular mesh is used in our simulation. The minimum unit is 1 nm, and the maximum unit is 2 μm. The resolution of the narrow region is set to 10 to ensure simulation accuracy. In our simulation, the device is surrounded by a 500 μm × 2000 μm air box with scattering boundary condition. Thanks to the high microwave/optical refractive index contrast between the BTO claddings and the MQW core, both the microwave and optical fields are well confined, as illustrated by Figs. 2(e) and 2(f). The electric field loading efficiency and the optical confinement factor of the membrane modulator are estimated to be 90.2% and 91.6%, respectively. In comparison, the n-i-p-n modulator exhibits an electric field loading efficiency of 84.3%, but a

Optics EXPRESS

much lower optical confinement factor of only 67.3%. The free carrier absorption loss due to the evanescent optical field in the doped InP claddings is simulated to be 1.3 dB/cm. In contrast, free carrier absorption induced optical loss is expected to be negligible in the proposed membrane MQW modulator. As a result of the tight optical confinement in the MQW core and relatively low absorption loss of BTO at near infrared [30], the optical absorption loss caused by the BTO claddings is estimated to be only 0.5 dB/cm.

4.2. Modulation efficiency

As shown in Fig. 1(a), the proposed modulator is designed with a feeder section, and the microwave modulation signal can be fed to the modulator through a ground-signal (GS) microwave probe. The bottom electrode is connected to the DC bias via a DC probe. Thus, a DC bias voltage can be applied to both arms of the modulator. Figure 5(a) shows the circuit schematic of the modulator, and the electric field loading is the same as in Ref. [31]. The modulation efficiency is characterized by the half-wave voltage-length product $V_\pi L$, which is given by [31]:

$$V_\pi L = \frac{\lambda}{\eta n_{eff}^3} \frac{1}{[r_{41}\Gamma_L/h_{MQW} + 2R\Gamma_Q V_B/h_{MQW}^2]}, \tag{1}$$

where λ = 1550 nm is the operating wavelength, η is the duty cycle of the T-rails, r_{41} = 1.0 pm/V and R = 1.4×10^{-19} m^2/V^2 are the linear and quadratic EO coefficients of the MQW core [1], n_{eff} is the effective refractive index of the optical mode and V_B is the bias voltage. Γ_L and Γ_Q are the linear and quadratic EO overlap factors, given as follows [32]:

$$\Gamma_L = \iint \frac{E_z}{V/h_{MQW}} |\gamma|^2 dS, \tag{2}$$

$$\Gamma_Q = \iint \frac{E_z^2}{(V/h_{MQW})^2} |\gamma|^2 dS, \tag{3}$$

γ is the optical confinement factor, and V is the modulation voltage. EO interaction in the membrane MQW modulator is significantly enhanced by the strong optical confinement, and Γ_L and Γ_Q are calculated to be 80.7% and 72.0%, respectively. The variation of $V_\pi L$ with the applied bias voltage V_B calculated with Eq. (1) is plotted in Fig. 5. The half-wave voltage-length product $V_\pi L$ of the membrane MQW modulator is 0.45 V·cm under a bias voltage of 10 V. For the n-i-p-n modulator reported in Ref. [23], $V_\pi L$ is 0.6 V·cm under the same bias voltage. $V_\pi L$ can be effectively reduced by further increasing the bias voltage. However, an excessively high bias voltage may lead to breakdown of the n-i-p-n modulator, which relies on the reversely biased p-n junction to block leakage current. In contrast, the breakdown voltage of the BTO claddings in the membrane modulator is as high as 1.2×10^6 V/cm [29], thus allowing a higher bias voltage. A $V_\pi L$ of only 0.24 V·cm is estimated for the membrane MQW modulator at a bias voltage of 20 V. For the device with a modulation length of 2 mm, the half-wave voltage V_π is as low as 1.2 V.

4.3. Modulation bandwidth

The microwave S-parameters of the membrane MQW modulator with a 2 mm modulation length obtained by FEM with lumped port excitation and radiation boundary are plotted Fig. 6(a). The microwave reflection S_{11} remains below −15 dB up to 300 GHz, implying satisfactory impedance matching. The 6.34-dB bandwidth of the microwave transmission S_{21} is over 240 GHz, indicating a greatly reduced microwave propagation loss. The extracted microwave refractive index in Fig. 6(b) shows excellent match with the optical group index (~3.5). Meanwhile, the characteristic impedance given in Fig. 6(c) is close to 50 Ω.

For an MZM with perfect impedance and velocity matching, the 3-dB EO modulation bandwidth depends on the microwave loss, and corresponds to the 6.34-dB bandwidth of the

Optics EXPRESS

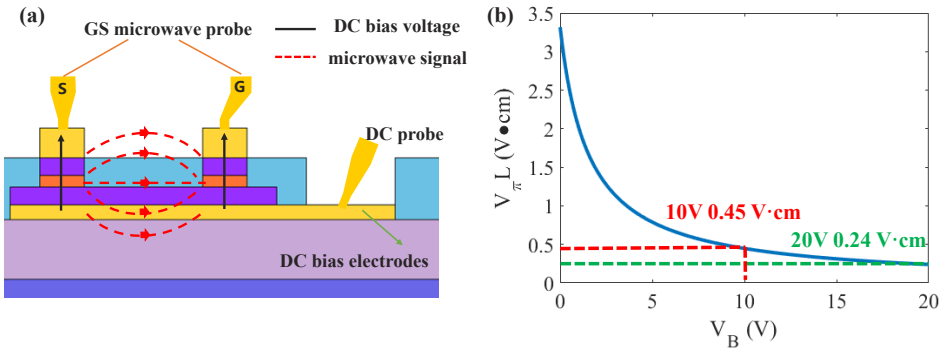

Fig. 5. (a) Circuit schematic and (b) half-wave voltage-length product of the membrane MQW modulator under different bias voltages.

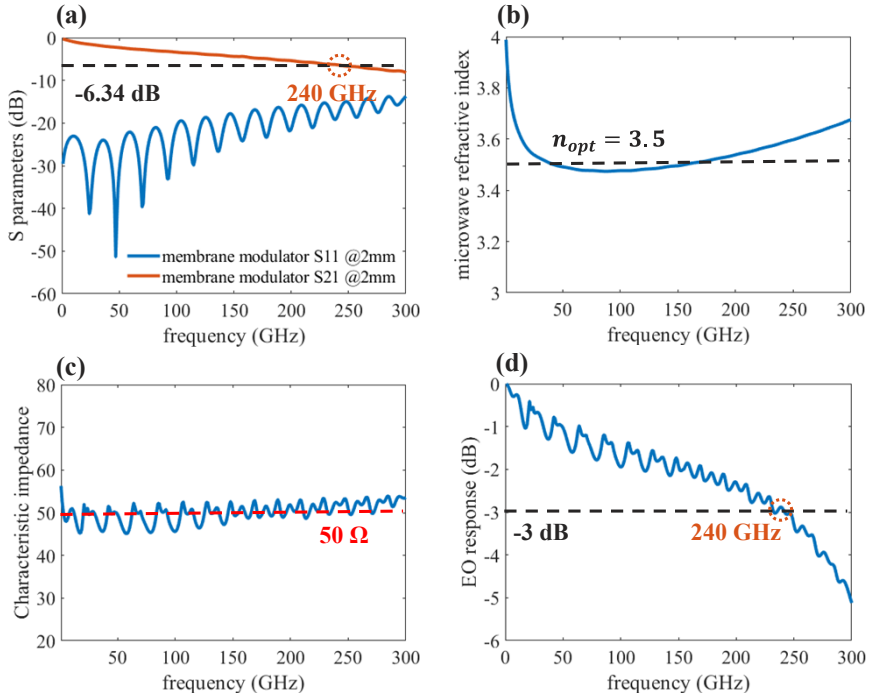

Fig. 6. (a) Simulated S-parameters, (b) extracted microwave refractive index, (c) characteristic impedance and (d) EO response of the membrane MQW modulator.

Optics EXPRESS

microwave transmission S_{21} [31]. In order to accurately estimate the EO frequency response of the membrane modulator, the impedance and velocity mismatch as well as the microwave transmission loss are taken into account via a full-wave simulation [33]. As the length of the T-rails is much smaller than the microwave wavelength, the CL-TWEs can be modelled as lumped elements connected by the main electrodes. According to the transmission line model, the average effective loaded voltage along the modulation length L at modulation frequency ω can be expressed as [33]:

$$V_{avg}(\omega) = \frac{1}{L}\sum_{i=1}^{N}\frac{V_g}{2}(1+\rho_1)e^{i\beta_o L}\frac{e^{i(\beta_e-\beta_o)(i-\frac{1}{2})L_p}+\rho_2 e^{-i(\beta_e+\beta_o)(i-\frac{1}{2})L_p}}{e^{i\beta_e L}+\rho_1\rho_2 e^{-i\beta_e L}}L_{act}, \tag{4}$$

where N is the total number of T-rails, V_g is the amplitude of driving voltage, L is the length of the modulation region, L_p is the period of the CL-TWE, L_{act} is the effective modulation length of one cycle, $\beta_e - \beta_o$ and $\beta_e + \beta_o$ represent the wave vector walk-off between the optical and the transmitted/reflected microwave signals, respectively, while ρ_1 and ρ_2 represent the input/output reflection coefficients of the microwave transmission line. The EO responses of the proposed membrane MQW EO modulator is shown in Fig. 6(d). The 3-dB EO bandwidth of the modulator is similar to the 6.34-dB bandwidth of the S_{21} curve shown in Fig. 6(a), confirming nearly perfect impedance and velocity matching. A modulation bandwidth as high as 240 GHz is predicted for the proposed membrane MQW modulator with a 2 mm modulation length.

5. Conclusion

In conclusion, a membrane MQW EO modulator based on high-k material is proposed. By employing BTO in place of doped InP claddings, the microwave propagation loss and optical absorption loss can be significantly reduced. The membrane MQW modulator exhibits a high modulation efficiency, and a half-wave voltage length product $V_\pi L$ of only 0.24 V·cm is expected. A 2-mm-long membrane modulator is estimated to exhibit a half-wave voltage of 1.2 V and a large theoretical modulation bandwidth over 240 GHz. The performances of different modulators based on TFLN and InP are summarized in Table 2.

Table 2. Performance comparison of different modulators.

Material	Ref.	$V_\pi \cdot L$	E-O bandwidth	V_π
TFLN	[2]	1.7 V·cm	>67 GHz @ 5 mm	3.4 V
	[13]	2.8 V·cm	45 GHz @ 20 mm	1.4 V
		2.3 V·cm	80 GHz @ 10 mm	2.3 V
		2.2 V·cm	100 GHz @ 5 mm	4.4 V
	[14]	2.2 V·cm	>70 GHz @ 3 mm	7.4 V
		2.5 V·cm	70 GHz @ 5 mm	5.1 V
	[15]	1.75 V·cm	>40 GHz @ 5 mm	3.5 V
InP	[18]	0.38 V·cm	31 GHz @ 1.25 mm	3 V
	[19]	0.66 V·cm	40 GHz @ 3 mm	2.2 V
	[22]	0.6 V·cm	67 GHz @ 4 mm	1.5 V
	[23]	0.6 V·cm	80 GHz @ 4 mm	1.5 V
MQW with high-k material	This work	0.24 V·cm	240GHz @ 2 mm	1.2 V

The bandwidth-voltage limitations of InP-based and TFLN modulators are about 50 GHz/V and 140 GHz/V, respectively. In contrast, the proposed membrane MQW EO modulator is predicted to extend the limitation to 200 GHz/V with just 2-mm-long modulation region, demonstrating the capacity for sub-terahertz operation with a low half-wave voltage.

Optics EXPRESS

Compared with traditional InP-based EO modulators, the main challenges faced by the proposed membrane modulator lie in the preparation of high quality BTO claddings and the transfer-print of the MQW core. So far BTO film with fairly good quality has been prepared by RF magnetron sputtering [30]. Currently, wafer scale transfer-print remains a challenge and the quality of bonding between BTO and III-V materials is sensitive to lattice mismatch and surface charges of the strong ferroelectric. Nevertheless, with the progress in transfer-print techniques for heterogeneous integration of photonic components [25], it is believed the challenges faced by the proposed structure can be solved eventually, allowing substantial improvement in device performances.

Funding. Collaborative Innovation Centre of Solid-State Lighting and Energy-Saving Electronics; China Postdoctoral Science Foundation (2019T120090); Key Lab Program of BNRist (BNR2019ZS01005); National Natural Science Foundation of China (61822404, 61875104, 61904093, 61927811, 61974080, 61975093, 61991443); National Key Research and Development Program of China (2018YFB2201701).

Disclosures. The authors declare no conflicts of interest.

Data availability. Data underlying the results presented in this paper are not publicly available at this time but may be obtained from the authors upon reasonable request.

References

1. X. Zhao, B. Xiong, C. Sun, and Y. Luo, "Low drive voltage optical phase modulator with novel InGaAlAs/InAlAs multiple-quantum-barrier based n-i-n heterostructure," Opt. Express **21**(21), 24894–24903 (2013).
2. X. Liu, B. Xiong, C. Sun, J. Wang, Z. Hao, L. Wang, Y. Han, H. Li, J. Yu, and Y. Luo, "Wideband thin-film lithium niobate modulator with low half-wave-voltage length product," Chin. Opt. Lett. **19**(6), 060016 (2021).
3. J. Xing, C. Sun, C. Sun, B. Xiong, B. Xiong, J. Wang, J. Wang, Z. Hao, Z. Hao, L. Wang, Y. Han, Y. Han, Y. Han, H. Li, J. Yu, Y. Luo, Y. Luo, and Y. Luo, "Low loss hybrid plasmon polariton Mach-Zehnder modulators," OSA Continuum **4**(11), 2721–2733 (2021).
4. D. Marpaung, J. Yao, and J. Capmany, "Integrated microwave photonics," Nat. Photonics **13**(2), 80–90 (2019).
5. M. Burla, C. Hoessbacher, W. Heni, C. Haffner, Y. Fedoryshyn, D. Werner, T. Watanabe, H. Massler, D. L. Elder, L. R. Dalton, and J. Leuthold, "500 GHz plasmonic Mach-Zehnder modulator enabling sub-THz microwave photonics," APL Photonics **4**(5), 056106 (2019).
6. C. Haffner, W. Heni, Y. Fedoryshyn, J. Niegemann, A. Melikyan, D. L. Elder, B. Baeuerle, Y. Salamin, A. Josten, U. Koch, C. Hoessbacher, F. Ducry, L. Juchli, A. Emboras, D. Hillerkuss, M. Kohl, L. R. Dalton, C. Hafner, and J. Leuthold, "All-plasmonic Mach–Zehnder modulator enabling optical high-speed communication at the microscale," Nat. Photonics **9**(8), 525–528 (2015).
7. C. Haffner, W. Heni, D. L. Elder, Y. Fedoryshyn, N. Đorđević, D. Chelladurai, U. Koch, K. Portner, M. Burla, B. Robinson, L. R. Dalton, and J. Leuthold, "Harnessing nonlinearities near material absorption resonances for reducing losses in plasmonic modulators," Opt. Mater. Express **7**(7), 2168–2181 (2017).
8. T. Baba, S. Akiyama, M. Imai, and T. Usuki, "25-Gb/s broadband silicon modulator with 0.31-V·cm $V_{\pi}L$ based on forward-biased PIN diodes embedded with passive equalizer," Opt. Express **23**(26), 32950–32960 (2015).
9. D. J. Thomson, F. Y. Gardes, Y. Hu, G. Mashanovich, M. Fournier, P. Grosse, J.-M. Fedeli, and G. T. Reed, "High contrast 40Gbit/s optical modulation in silicon," Opt. Express **19**(12), 11507–11516 (2011).
10. X. Xiao, H. Xu, X. Li, Z. Li, T. Chu, Y. Yu, and J. Yu, "High-speed, low-loss silicon Mach–Zehnder modulators with doping optimization," Opt. Express **21**(4), 4116–4125 (2013).
11. S. Jain, S. Rajput, V. Kaushik, and M. Kumar, "High speed optical modulator based on silicon slotted-rib waveguide," Opt. Commun. **434**, 49–53 (2019).
12. M. Streshinsky, R. Ding, Y. Liu, A. Novack, Y. Yang, Y. Ma, X. Tu, E. K. S. Chee, A. E.-J. Lim, P. G.-Q. Lo, T. Baehr-Jones, and M. Hochberg, "Low power 50 Gb/s silicon traveling wave Mach-Zehnder modulator near 1300 nm," Opt. Express **21**(25), 30350–30357 (2013).
13. C. Wang, M. Zhang, X. Chen, M. Bertrand, A. Shams-Ansari, S. Chandrasekhar, P. Winzer, and M. Lončar, "Integrated lithium niobate electro-optic modulators operating at CMOS-compatible voltages," Nature **562**(7725), 101–104 (2018).
14. M. He, M. Xu, Y. Ren, J. Jian, Z. Ruan, Y. Xu, S. Gao, S. Sun, X. Wen, L. Zhou, L. Liu, C. Guo, H. Chen, S. Yu, L. Liu, and X. Cai, "High-performance hybrid silicon and lithium niobate Mach–Zehnder modulators for 100 Gbit s−1 and beyond," Nat. Photonics **13**(5), 359–364 (2019).
15. Y. Liu, H. Li, J. Liu, S. Tan, Q. Lu, and W. Guo, "Low V_{π} thin-film lithium niobate modulator fabricated with photolithography," Opt. Express **29**(5), 6320–6329 (2021).
16. A. J. Mercante, S. Shi, P. Yao, L. Xie, R. M. Weikle, and D. W. Prather, "Thin film lithium niobate electro-optic modulator with terahertz operating bandwidth," Opt. Express **26**(11), 14810–14816 (2018).
17. M. Xu, M. He, H. Zhang, J. Jian, Y. Pan, X. Liu, L. Chen, X. Meng, H. Chen, Z. Li, X. Xiao, S. Yu, S. Yu, and X. Cai, "High-performance coherent optical modulators based on thin-film lithium niobate platform," Nat. Commun. **11**(1), 3911 (2020).

Optics EXPRESS

18. G. Qian, B. Niu, W. Zhao, Q. Kan, X. Gu, F. Zhou, Y. Kong, and T. Chen, "CL-TWE Mach–Zehnder electro-optic modulator based on InP-MQW optical waveguides," Chin. Opt. Lett. **17**(6), 061301 (2019).
19. K. Tsuzuki, T. Ishibashi, T. Ito, S. Oku, Y. Shibata, T. Ito, R. Iga, Y. Kondo, and Y. Tohmori, "A 40-gb/s InGaAlAs-InAlAs MQW n-i-n Mach-Zehnder Modulator with a drive Voltage of 2.3 V," IEEE Photonics Technol. Lett. **17**(1), 46–48 (2005).
20. S. Akiyama, H. Itoh, T. Takeuchi, A. Kuramata, and T. Yamamoto, "Wide-wavelength-band (30 nm) 10-Gb/s operation of InP-based Mach-Zehnder modulator with constant driving voltage of 2 V_{pp}," IEEE Photonics Technol. Lett. **17**(7), 1408–1410 (2005).
21. H. Yasaka, K. Tsuzuki, N. Kikuchi, N. Ishikawa, T. Yasui, and Y. Shibata, "Advances in InP Mach-Zehnder modulators for large capacity photonic network systems," in *2008 20th International Conference on Indium Phosphide and Related Materials* (2008), pp. 1–5.
22. Y. Ogiso, J. Ozaki, Y. Ueda, N. Kashio, N. Kikuchi, E. Yamada, H. Tanobe, S. Kanazawa, H. Yamazaki, Y. Ohiso, T. Fujii, and M. Kohtoku, "Over 67 GHz Bandwidth and 1.5 V Vπ InP-Based Optical IQ Modulator With n-i-p-n Heterostructure," J. Lightwave Technol. **35**(8), 1450–1455 (2017).
23. Y. Ogiso, J. Ozaki, Y. Ueda, H. Wakita, M. Nagatani, H. Yamazaki, M. Nakamura, T. Kobayashi, S. Kanazawa, Y. Hashizume, H. Tanobe, N. Nunoya, M. Ida, Y. Miyamoto, and M. Ishikawa, "80-GHz Bandwidth and 1.5-V V_π InP-Based IQ Modulator," J. Lightwave Technol. **38**(2), 249–255 (2020).
24. J. Xing, C. Sun, B. Xiong, J. Wang, Z. Hao, L. Wang, Y. Han, H. Li, J. Yu, and Y. Luo, "Membrane Multiple Quantum Well Electro-Optical Modulator Based on High-k Material," in *Asia Communications and Photonics Conference 2021* (2021), p. T4A.179.
25. B. Corbett, R. Loi, W. Zhou, D. Liu, and Z. Ma, "Transfer print techniques for heterogeneous integration of photonic components," Prog. Quantum Electron. **52**, 1–17 (2017).
26. Y. Liu, L. Wang, L. Wang, X. Wu, Z. Hao, J. Yu, Y. Luo, C. Sun, Y. Han, B. Xiong, J. Wang, and H. Li, "A p-Si/n-GaN diode fabricated by nanomembrane lift-off and transfer-print technique," Semicond. Sci. Technol. **34**(10), 105023 (2019).
27. J.-H. Han, F. Boeuf, J. Fujikata, S. Takahashi, S. Takagi, and M. Takenaka, "Efficient low-loss InGaAsP/Si hybrid MOS optical modulator," Nat. Photonics **11**(8), 486–490 (2017).
28. X. Guo, A. He, and Y. Su, "Recent advances of heterogeneously integrated III–V laser on Si," J. Semicond. **40**(10), 101304 (2019).
29. Z. Q. Shi, Q. X. Jia, and W. A. Anderson, "Electrical and dielectric properties of thin film BaTiO3 capacitors deposited by radio frequency magnetron sputtering," J. Vac. Sci. Technol., A **10**(4), 733–736 (1992).
30. S. Ummethala, J. N. Kemal, A. S. Alam, M. Lauermann, A. Kuzmin, Y. Kutuvantavida, S. H. Nandam, L. Hahn, D. L. Elder, L. R. Dalton, T. Zwick, S. Randel, W. Freude, and C. Koos, "Hybrid electro-optic modulator combining silicon photonic slot waveguides with high-k radio-frequency slotlines," Optica **8**(4), 511–519 (2021).
31. H. Chen, "Development of an 80 Gbit/s InP-based Mach-Zehnder Modulator," Doctoral Thesis, Technical University Berlin (2007).
32. H. Klein, "Integrated InP Mach-Zehnder Modulators for 100 Gbit/s Ethernet Applications using QPSK Modulation," Doctoral Thesis, Technical University Berlin (2010).
33. S. H. Lin and S.-Y. Wang, "High-throughput GaAs PIN electrooptic modulator with a 3-dB bandwidth of 9.6 GHz at 1.3 μm," Appl. Opt. **26**(9), 1696–1700 (1987).